

AKADEMIA GÓRNICZO-HUTNICZA IM. STANISŁAWA STASZICA W KRAKOWIE

FACULTY OF MECHANICAL ENGINEERING AND ROBOTICS

Master's thesis

Quaternions in mathematical modeling of rotary machines

Autor: *Eng. Maciej Posłuszny*
Kierunek studiów: *Mechanical Engineering*
Opiekun pracy: *PhD Eng. Sebastian Pakuła*

Kraków, 15.07.2026

Uprzedzony o odpowiedzialności karnej na podstawie art. 115 ust. 1 i 2 ustawy z dnia 4 lutego 1994 r. o prawie autorskim i prawach pokrewnych (t.j. Dz.U. z 2006 r. Nr 90, poz. 631 z późn. zm.): „Kto przywłaszcza sobie autorstwo albo wprowadza w błąd co do autorstwa całości lub części cudzego utworu albo artystycznego wykonania, podlega grzywnie, karze ograniczenia wolności albo pozbawienia wolności do lat 3. Tej samej karze podlega, kto rozpowszechnia bez podania nazwiska lub pseudonimu twórcy cudzy utwór w wersji oryginalnej albo w postaci opracowania, artystycznego wykonania albo publicznie zniekształca taki utwór, artystyczne wykonanie, fonogram, wideogram lub nadanie.”, a także uprzedzony o odpowiedzialności dyscyplinarnej na podstawie art. 211 ust. 1 ustawy z dnia 27 lipca 2005 r. Prawo o szkolnictwie wyższym (t.j. Dz. U. z 2012 r. poz. 572, z późn. zm.): „Za naruszenie przepisów obowiązujących w uczelni oraz za czyny uchybiające godności studenta student ponosi odpowiedzialność dyscyplinarną przed komisją dyscyplinarną albo przed sądem koleżeńskim samorządu studenckiego, zwanym dalej «sądem koleżeńskim».”, oświadczam, że niniejszą pracę dyplomową wykonałem(-am) osobiście i samodzielnie i że nie korzystałem(-am) ze źródeł innych niż wymienione w pracy.

I would like to express my sincere gratitude to my supervisor, PhD Eng. Sebastian Pakuła, for his invaluable guidance and support throughout the preparation and writing of this thesis.

Spis treści

1. Introduction 7

1.1. Background 7

1.2. Aim and Scope of the Thesis 8

2. Euler Angles 9

2.1. Definition of Euler Angles 9

2.2. Problems Associated with Euler Angles 11

3. Quaternions 12

3.1. Definition of a Quaternion 12

3.2. Basic Algebraic Properties 13

3.3. Quaternion Kinematics Equation 14

3.4. Limitations of Quaternions 15

4. Dual Quaternions 16

4.1. Dual Numbers 16

4.2. Algebra of Dual Quaternions 16

4.3. Applications of Dual Quaternions 18

5. Kinematics and Dynamics Modeling of a Spinning Top 19

5.1. Kinematic Model 19

5.2. Analytical Solution — Euler Angles 20

5.2.1. System's Energy 20

5.2.2. Dynamics Equations 22

5.3. Analytical Solution — Quaternion Representation 23

5.3.1. Kinematic Equations 23

5.3.2. Dynamic Equations 24

5.4. Numerical Computations 26

5.4.1. Comparison of Time Histories 26

5.4.2. Comparison of Computation Time 28

5.4.3. Analysis of Results 29

6. Kinematics and Dynamics Modeling of a Rotor 30
6.1. Kinematic Model of the System 30
6.2. Analytical Solution — Euler Angles 32
6.2.1. Rotor Kinematics 32
6.2.2. Dynamics Equations 32
6.3. Analytical Solution — Dual Quaternion Representation 33
6.3.1. Kinematic Equations of the Model 34
6.3.2. Rotational Motion Equations 34
6.3.3. Translational Motion Equations 35
6.4. Numerical Computations 37
6.4.1. Comparison of Time Histories 38
6.4.2. Comparison of Computation Time 39
6.4.3. Analysis of Results 39
7. Summary 40

1. Introduction

1.1. Background

The description of rigid-body motion is one of the fundamental topics in mechanics and in the mathematical modeling of technical systems. While the description of translational motion is relatively straightforward and requires specifying only the position of a material point, incorporating the spatial orientation of a body leads to a significant increase in the complexity of the mathematical model. Particularly demanding is the general motion, understood as the combination of translational and rotational motion. An object undergoing general motion possesses exactly six degrees of freedom (6 DOF), three of which correspond to translation and the remaining three to rotation.

To describe the orientation of a rigid body, Euler angles are most commonly used. They allow the orientation of a local coordinate system attached to the body to be uniquely defined with respect to a global reference frame through three successive rotations. This representation is widely used in mechanics, robotics, and machine dynamics due to its intuitive geometric interpretation and straightforward implementation. However, the method suffers from a significant drawback: the presence of representation singularities known as gimbal lock, which, for certain configurations, leads to the loss of one degree of freedom and consequently to numerical difficulties.

An alternative method for describing orientation is the use of quaternions. They represent spatial orientation using four parameters that form a quaternion, thereby eliminating the singularity problem characteristic of Euler angles. Moreover, quaternion-based orientation enables efficient computation of rotations and interpolation of orientations, making it useful in robotics, aviation, astronautics, and computer graphics.

An extension of quaternions is the dual quaternion formulation, which allows simultaneous representation of both the orientation and the position of a rigid body. This makes it possible to describe the full general motion of a body using a single mathematical object, without the need to separately represent translation and rotation. For this reason, dual quaternions are increasingly used in the modeling of mechanical systems and rotor machinery.

1.2. Aim and Scope of the Thesis

The subject of this thesis is the comparison of the classical description of rigid-body motion using Euler angles with quaternion-based and dual-quaternion-based formulations. The aim is to compare the classical and quaternion approaches in terms of motion-representation accuracy and computational efficiency, as well as to present the advantages of using quaternions in the mathematical modeling of objects undergoing spherical and general motion, with particular emphasis on unbalanced rotor machines. The computational analysis was carried out for two systems:

1. a symmetric spinning top performing spherical motion, described by three rotational degrees of freedom;

2. an unbalanced rotor supported elastically, performing constrained general motion, described by three rotational and two translational degrees of freedom, giving a total of five degrees of freedom.

For both models, analytical equations of motion were derived and subsequently implemented in MATLAB as simulation models solving systems of differential equations using the fourth-order Runge–Kutta method. Based on the derived equations, simulation models were developed to enable numerical analysis of the motion of both systems and to compare the classical and quaternion representations of orientation.

2. Euler Angles

Euler angles constitute a set of three angles that enable an unambiguous description of the relative orientation of two Cartesian coordinate systems sharing a common origin. Euler angles constitute a set of three angles that enable an unambiguous description of the relative orientation of two Cartesian coordinate systems sharing a common origin [1]. In the literature, one of these systems is typically considered the fixed global frame xyz, while the other represents the local frame $\xi\eta\zeta$ attached to a rotating rigid body [2]. The orientation of the local frame with respect to the global frame is described by a sequence of successive rotations about selected axes.

2.1. Definition of Euler Angles

Euler angles are most commonly expressed in the form of rotation matrices:

$$
\begin{aligned}
R_x(\alpha) &= \begin{bmatrix} 1 & 0 & 0 \\ 0 & \cos\alpha & -\sin\alpha \\ 0 & \sin\alpha & \cos\alpha \end{bmatrix} \coloneqq X_\alpha \\
R_y(\alpha) &= \begin{bmatrix} \cos\alpha & 0 & \sin\alpha \\ 0 & 1 & 0 \\ -\sin\alpha & 0 & \cos\alpha \end{bmatrix} \coloneqq Y_\alpha \\
R_z(\alpha) &= \begin{bmatrix} \cos\alpha & -\sin\alpha & 0 \\ \sin\alpha & \cos\alpha & 0 \\ 0 & 0 & 1 \end{bmatrix} \coloneqq Z_\alpha
\end{aligned}
\tag{2.1}
$$

where X_α, Y_α, and Z_α denote rotation matrices about the x, y,and z respectively, and α is the angle of rotation. The product of three appropriately selected rotation matrices yields the rotation matrix describing the orientation of the local frame relative to the global frame. There exist twelve possible rotation sequences, among which the following are distinguished:

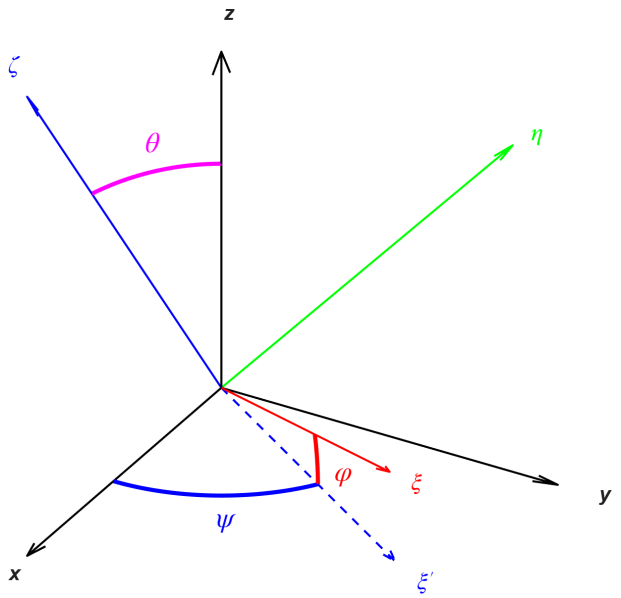
- **Six classical Euler angle sequences** in which the first and third rotation axes coincide, e.g. $X_\alpha Z_\beta X_\gamma$ or $Z_\alpha X_\beta Z_\gamma$;

– **Six Tait–Bryan sequences** (also known as Cardan angles), in which each rotation axis appears exactly once, e.g. $X_\alpha Y_\beta Z_\gamma$ or $Z_\alpha Y_\beta X_\gamma$. These sequences are widely used, particularly in aviation and spacecraft dynamics [3].

An example of a rotation sequence and a complete list of all possible combinations are presented below. In the remainder of this thesis, the sequences $Z_\alpha X_\beta Z_\gamma$ and $Z_\alpha Y_\beta X_\gamma$ are used.

classical Euler angles	**Tait–Bryan angles**
$X_\alpha Z_\beta X_\gamma$	$X_\alpha Y_\beta Z_\gamma$
$Z_\alpha X_\beta Z_\gamma$	$Z_\alpha Y_\beta X_\gamma$
$X_\alpha Y_\beta X_\gamma$	$X_\alpha Z_\beta Y_\gamma$
$Y_\alpha X_\beta Y_\gamma$	$Y_\alpha Z_\beta X_\gamma$
$Z_\alpha Y_\beta Z_\gamma$	$Y_\alpha X_\beta Z_\gamma$
$Y_\alpha Z_\beta Y_\gamma$	$Z_\alpha X_\beta Y_\gamma$

Tabela 2.1. All possible Euler angle multiplication sequences.



Rys. 2.1. Example of the rotation sequence $Z_\psi X_\theta Z_\varphi$ resulting in the orientation of the local coordinate system $\xi\eta\zeta$ with respect to the global system xyz, for $\psi, \theta, \varphi = 30°$. he first rotation is performed about the z-axis by the angle ψ, producing the line of nodes ξ', which is the intersection of the planes xy and $\xi\eta$. Next, a rotation by the angle θ, is carried out about this line, causing the ζ-axis to tilt relative to the z-axis. The final step is a rotation by the angle φ about the local ζ-axis, yielding the resulting orientation of the local coordinate system with respect to the global one.

2.2. Problems Associated with Euler Angles

The main advantages of Euler angles include their simplicity and intuitive geometric interpretation. Representing orientation through three successive rotations has been used for many years in mechanics and machine dynamics, and its mathematical framework is relatively straightforward. For this reason, Euler angles remain one of the most commonly used methods for describing the orientation of a rigid body. Despite their numerous advantages, this representation also has significant limitations. These include the need to select an appropriate rotation sequence, the presence of singularities, and limited convenience when performing calculations for complex systems [4].

The most serious drawback is the occurrence of the phenomenon known as *Gimbal Lock* [5]. This phenomenon arises when one of the Euler angles reaches a value corresponding to a singular configuration of the chosen rotation sequence, causing two rotation axes to align and the system to lose one degree of freedom. As a result, the orientation of the body can no longer be uniquely represented using Euler angles. This leads to difficulties in numerical simulations and in applications requiring continuous orientation tracking, such as computer graphics, navigation systems, or aircraft control. In computer animation and 3D graphics, gimbal lock may result in chaotic and unpredictable motion of animated objects.

Gimbal lock may also occur in navigation systems and is particularly dangerous in aviation and unmanned aerial vehicles. Near singular configurations of Euler angle representations, gyroscopic systems fail to provide unambiguous orientation information, which may lead to a loss of control over the vehicle. Historically, a gimbal refers to a system of rings—also known as a Cardan suspension—used in gyroscopes to support the rotor and allow rotation about three axes.

In practice, various methods are used to mitigate the effects of gimbal lock, such as changing the rotation sequence or switching to a different orientation representation. These solutions increase implementation complexity and do not eliminate the root cause of the problem. For this reason, many modern applications replace Euler angles with quaternion-based representations.

3. Quaternions

The concept of the quaternion was first introduced by Hamilton in the 19th century [5] [6]. Quaternions constitute an extension of complex numbers. They are composed of one real part and three imaginary parts, forming a four-dimensional linear space. In honor of their creator, the set of quaternions is denoted by Hamilton's symbol $\mathbb{H}$.

3.1. Definition of a Quaternion

A quaternion in its algebraic form is defined as:

$$\bar{q} = w + x\hat{i} + y\hat{j} + z\hat{k} \tag{3.1}$$

where $\hat{i}$, $\hat{j}$, and $\hat{k}$ denote the imaginary quaternion units corresponding to the three spatial directions. They satisfy the relations:

$$i^2 = j^2 = k^2 = -1 \tag{3.2}$$

and

$$\begin{aligned} ij &= k, \quad ji = -k \\ jk &= i, \quad kj = -i \\ ki &= j, \quad ik = -j \end{aligned} \tag{3.3}$$

as well as

$$i \neq j \neq k \tag{3.4}$$

The quantities w, x, y, and z are the real-valued components of the quaternion, with w representing its real part.

One geometric interpretation of a unit quaternion identifies its imaginary part with a vector in three-dimensional space. For a unit quaternion, the normalization condition implies that all admissible component values lie on the unit hypersphere in four-dimensional space. The imaginary part can therefore be interpreted as a point in three-dimensional space.

A quaternion is often written as the sum of a scalar part and a vector part:

$$\bar{q} = (w, \bar{v}) \tag{3.5}$$

where $\bar{v} = [x, y, z]$ is the vector part of the quaternion. This decomposition into real and imaginary components is particularly useful when performing quaternion multiplication, along with several other operations discussed later in this chapter.

3.2. Basic Algebraic Properties

To work effectively with quaternion algebra, it is necessary to define and describe the fundamental mathematical operations. The essential operations performed within the quaternion field are listed below [5]:

1. **Multiplication by a scalar**:
$$s\bar{q} = (sw, s\bar{v}) \tag{3.6}$$
where $s \in \mathbb{R}$;

2. **Addition of quaternions**:
$$\bar{q}_1 + \bar{q}_2 = (w_1 + w_2, \bar{v}_1 + \bar{v}_2) \tag{3.7}$$
where $\bar{q}_1 = (w_1, \bar{v}_1), \quad \bar{q}_2 = (w_2, \bar{v}_2)$;

3. **Multiplication of quaternions**:
$$\bar{q}_1\bar{q}_2 = (w_1w_2 - \bar{v}_1\bar{v}_2,\ w_1\bar{v}_2 + w_2\bar{v}_1 + (\bar{v}_1 \times \bar{v}_2)) \tag{3.8}$$

4. **Conjugate of a quaternion**:
$$\bar{q}^* = (w, -\bar{v}) \tag{3.9}$$

5. **The norm of a quaternion**:
$$\|\bar{q}\| = \sqrt{\bar{q}\bar{q}^*} \tag{3.10}$$

In this work, the primary focus is on the case of a normalized quaternion, i.e., a quaternion for which:

$$\|\bar{q}\| = 1 \tag{3.11}$$

The normalization condition ensures that the rotation represented by the quaternion preserves the length of the rotated vector.

3.3. Quaternion Kinematics Equation

The rotation of a vector described using a quaternion can be expressed as:

$$\bar{x}' = \bar{q}\bar{x}\bar{q}^* \tag{3.12}$$

This is the standard equation describing the rotation of a vector x, commonly used in the differential kinematics of rigid bodies [7]. Differentiating the equation (3.12) yields [8]:

$$\dot{\bar{x}}' = \frac{d}{dt}(\bar{q}\bar{x}\bar{q}^*) = \dot{\bar{q}}\bar{x}\bar{q}^* + \bar{q}\bar{x}\dot{\bar{q}}^* \tag{3.13}$$

Using the normalization condition (3.11), we obtain:

$$\dot{\bar{x}} = \dot{\bar{q}}(\bar{q}^*\bar{q})\bar{x}\bar{q}^* + \bar{q}\bar{x}(\bar{q}^*\bar{q})\dot{\bar{q}}^* = \dot{\bar{q}}\bar{q}^*(\bar{q}\bar{x}\bar{q}^*) + (\bar{q}\bar{x}\bar{q}^*)\bar{q}\dot{\bar{q}}^* \tag{3.14}$$

Substituting relation 3.12 into equation 3.14 gives:

$$\dot{\bar{x}} = \dot{\bar{q}}\bar{q}^*\bar{x}' + \bar{x}'\bar{q}\dot{\bar{q}}^* \tag{3.15}$$

From the conjugation identity (3.9), it follows that:

$$\frac{d}{dt}(\bar{q}\bar{q}^*) = \dot{\bar{q}}\bar{q}^* + \bar{q}\dot{\bar{q}}^* = 0 \implies \bar{q}\dot{\bar{q}}^* = -\dot{\bar{q}}\bar{q}^* \tag{3.16}$$

Inserting this relation into equation 3.15 yields:

$$\dot{\bar{x}} = \dot{\bar{q}}\bar{q}^*\bar{x}' - \bar{x}'\dot{\bar{q}}\bar{q}^* = \bar{\Omega}\bar{x}' - \bar{x}'\bar{\Omega} \tag{3.17}$$

where $\bar{\Omega} \coloneqq \dot{\bar{q}}\bar{q}^*$.

Using the properties of quaternion multiplication (3.8) in the body-fixed frame, the following identity holds [7]:

$$\bar{\Omega}\bar{x}' - \bar{x}'\bar{\Omega} = (-\bar{\Omega}\cdot\bar{x}' - (-\bar{\Omega}\cdot\bar{x}'), \bar{\Omega}\times\bar{x}' + \bar{\Omega}\times\bar{x}') = (0, 2\bar{\Omega}\times\bar{x}') \tag{3.18}$$

Furthermore, according to classical mechanics [2], the derivative of the vector x' in the rotational motion of a rigid body satisfies:

$$\dot{\bar{x}}' = \bar{\omega}\times\bar{x}' \tag{3.19}$$

where $\bar{\omega}$ is the angular velocity of the rotational motion. The angular-velocity vector can be represented as a quaternion by mapping its three components to the imaginary coordinates and adding a real part equal to zero. Thus, relation 3.19 can be written as:

$$\dot{x}' = \bar{\omega}_q\times\bar{x}' = (0, \bar{\omega}_q\times\bar{x}') \tag{3.20}$$

where $\bar{\omega}_q = [0, \bar{\omega}]^T$. Comparing equations 3.18 and 3.20, we obtain:

$$\bar{\Omega} = \frac{1}{2}\bar{\omega}_q \tag{3.21}$$

Finally, the quaternion kinematics equation is obtained:

$$\dot{\bar{q}} = \frac{1}{2}\bar{\omega}_q \bar{q} \tag{3.22}$$

Equation 3.22 forms the basis for implementing the quaternion-based model used in this work. In contrast to the Euler-angle approach, where the state variables are the angles describing successive rotations, the quaternion model integrates the quaternion components and the angular velocity of the body directly. This allows the orientation to be determined continuously, without singularities in the representation.

3.4. Limitations of Quaternions

Quaternions express rotation as an angle about a specified axis, which in many cases provides a far more intuitive and natural way of representing spatial orientation than the more intricate operations involving Euler angles [4]. In contrast to Euler angles, quaternions do not require selecting a sequence of rotations and are particularly useful for orientation interpolation and object animation. They also allow for efficient numerical implementation. Moreover, they offer simple interpolation methods, enabling an elegant formulation of smooth transitions, and they support more computationally efficient numerical procedures. Their greatest advantage is undoubtedly the absence of gimbal lock, which makes them robust against singularities in the representation.

Nevertheless, the method is not without limitations. The fundamental constraint of quaternions is that they describe only the orientation of a rigid body. To represent both orientation and position simultaneously, an extended representation is required. This issue is addressed by dual quaternions, which enable the combined description of translation and rotation within a single algebraic entity.

4. Dual Quaternions

Dual quaternions are an extension of classical quaternions, constructed on the basis of dual-number algebra. For this reason, before discussing their properties, it is necessary to present the fundamental concepts related to dual numbers, which form the foundation for the construction of dual quaternions.

4.1. Dual Numbers

A dual number is defined as an element composed of two components: a real component $\mathbb{R}$ and a dual component $\mathbb{D}$ [9]. A dual number is written in the form:

$$\hat{a} = a_r + \varepsilon a_d \tag{4.1}$$

where $a_r, a_d \in \mathbb{R}$, $\varepsilon \in \mathbb{D}$. The quantity a_r is the real part of the dual number, while a_d is its dual part. The symbol ε denotes the dual unit, which satisfies $\varepsilon^2 = 0$ but $\varepsilon \neq 0$. Given two dual numbers of the form $\hat{a} = a_r + \varepsilon a_d$ and $\hat{b} = b_r + \varepsilon b_d$, their algebraic relations can be written as follows:

1. **Equality**:
$$\hat{a} = \hat{b} \iff a_r = b_r \wedge a_d = b_d, \tag{4.2}$$

2. **Addition**:
$$\hat{a} + \hat{b} = (a_r + \varepsilon a_d) + (b_r + \varepsilon b_d) = (a_r + b_r) + \varepsilon(a_d + b_d), \tag{4.3}$$

3. **Multiplication**:
$$\hat{a}\hat{b} = (a_r + \varepsilon a_d)(b_r + \varepsilon b_d) = a_r b_r + \varepsilon(a_r b_d + a_d b_r), \tag{4.4}$$

4. **Division**:
$$\frac{\hat{a}}{\hat{b}} = \frac{a_r + \varepsilon a_d}{b_r + \varepsilon b_d} = \frac{a_r}{b_r} + \varepsilon\left(\frac{a_d}{b_r} - \frac{a_r b_d}{b_r^2}\right), \tag{4.5}$$
Assuming that $b_r \neq 0$.

4.2. Algebra of Dual Quaternions

By combining the algebra of dual numbers with quaternion algebra, one obtains dual quaternions, first introduced by Clifford in 1882 [5]. In contrast to classical quaternions, which describe only the orientation of a rigid body, dual quaternions are capable of representing both rotational and translational motion.

A dual quaternion consists of a real part and a dual part, each of which is itself a quaternion. Mathematically, it is written as:

$$\hat{q} = \bar{q}_r + \varepsilon \bar{q}_d \tag{4.6}$$

As noted in the previous subsection, $\varepsilon^2 = 0$ and $\varepsilon \neq 0$. The term $\bar{q}_r$ is the real component that simultaneously represents the rotation quaternion of the object. The dual part $\bar{q}_d$ contains information about translation, and its value depends on the orientation described by the real part according to:

$$\bar{q}_d = \frac{1}{2} \bar{q}_{tr} \bar{q}_r^* \tag{4.7}$$

where $\bar{q}_{tr}$ is a purely imaginary translation quaternion describing the displacement vector [9].

The basic algebraic operations on dual quaternions are analogous to those presented in subsection 4.1:

1. **Multiplication by a scalar**:
$$s\hat{q} = s\bar{q}_r + s\varepsilon \bar{q}_d \tag{4.8}$$
where s is a scalar;

2. **Addition**:
$$\hat{q}_1 + \hat{q}_2 = \bar{q}_{r,1} + \bar{q}_{r,2} + \varepsilon(\bar{q}_{d,1} + \bar{q}_{d,2}) \tag{4.9}$$
where $\hat{q}_1 = \bar{q}_{r,1} + \varepsilon \bar{q}_{d,1}, \quad \hat{q}_2 = \bar{q}_{r,2} + \varepsilon \bar{q}_{d,2}$;

3. **Multiplication**:
$$\hat{q}_1 \hat{q}_2 = \bar{q}_{r,1}\bar{q}_{r,2} + \varepsilon(\bar{q}_{r,1}\bar{q}_{d,2} + \bar{q}_{r,2}\bar{q}_{d,1}) \tag{4.10}$$

4. **Conjugation**:
$$\hat{q}^* = \bar{q}_r^* + \varepsilon \bar{q}_d^* \tag{4.11}$$

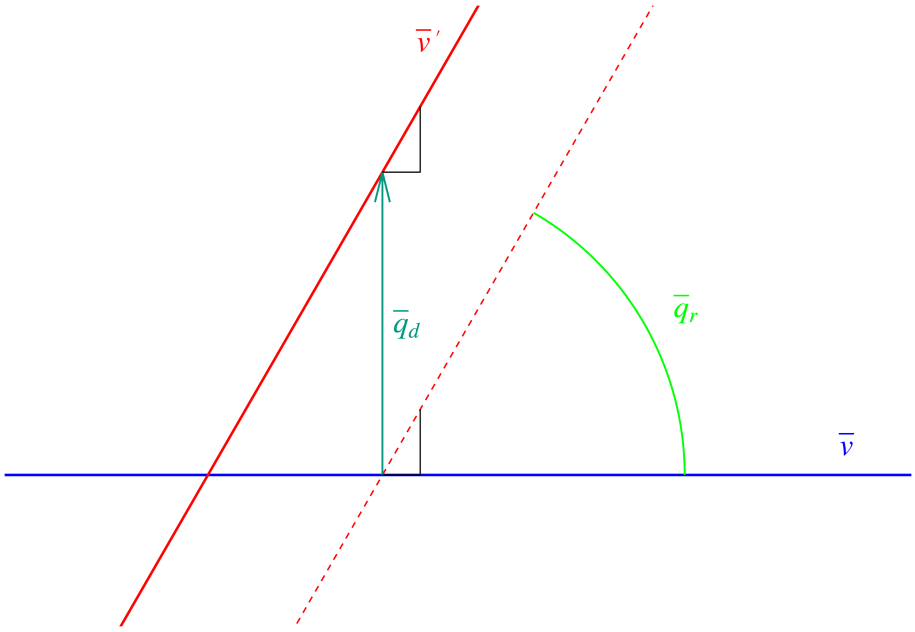
5. **Norm**:
$$\|\hat{q}\| = \hat{q}\hat{q}^* \tag{4.12}$$

6. **Normalization**:
$$\|\hat{q}\| = 1 \iff \bar{q}_r^* \bar{q}_d + \bar{q}_r \bar{q}_d^* = 0 \tag{4.13}$$
The normalization condition ensures that a dual quaternion represents a valid rigid-body transformation, encompassing both rotation and translation.

4.3. Applications of Dual Quaternions

A dual quaternion eliminates the fundamental limitation of a classical quaternion, namely its ability to describe only the orientation of a rigid body. A dual quaternion enables the simultaneous representation of both the position and orientation of a rigid body, which is why it is widely used in rigid-body dynamics in fields such as robotics [10], aeronautics and astronautics [11], and even biomedical engineering [12].

Moreover, the action of a dual quaternion can be interpreted geometrically in a straightforward manner. The component $\bar{q}_r$ in equation 4.6 describes the orientation of the body, whereas the component$\bar{q}_d$ corresponds to the translation of the system [9].



Rys. 4.1. An example visualization of a vector transformation using a dual quaternion. The dashed line indicates the axis resulting from the pure rotation of the vector $\bar{v}$.

The figure presents an example of how a transformation described by a dual quaternion can be interpreted. In the first stage, the real part of the dual quaternion $\bar{q}_r$ describes the rotation of the vector $\bar{v}$ about a specified axis. This operation yields an intermediate position, indicated in the figure by the dashed line. Next, the dual part $\bar{q}_d$ introduces the translational component, determined by the chosen displacement vector. This translation shifts the rotated vector to its final position. In this way, a dual quaternion enables the simultaneous representation of two operations: the rotation encoded in $\bar{q}_r$ and the translation encoded in $\bar{q}_d$.

Thanks to their ability to represent translation and rotation within a single algebraic object, dual quaternions have become one of the most commonly used representations in robotics, computer graphics, and mechanical system modeling.

5. Kinematics and Dynamics Modeling of a Spinning Top

5.1. Kinematic Model

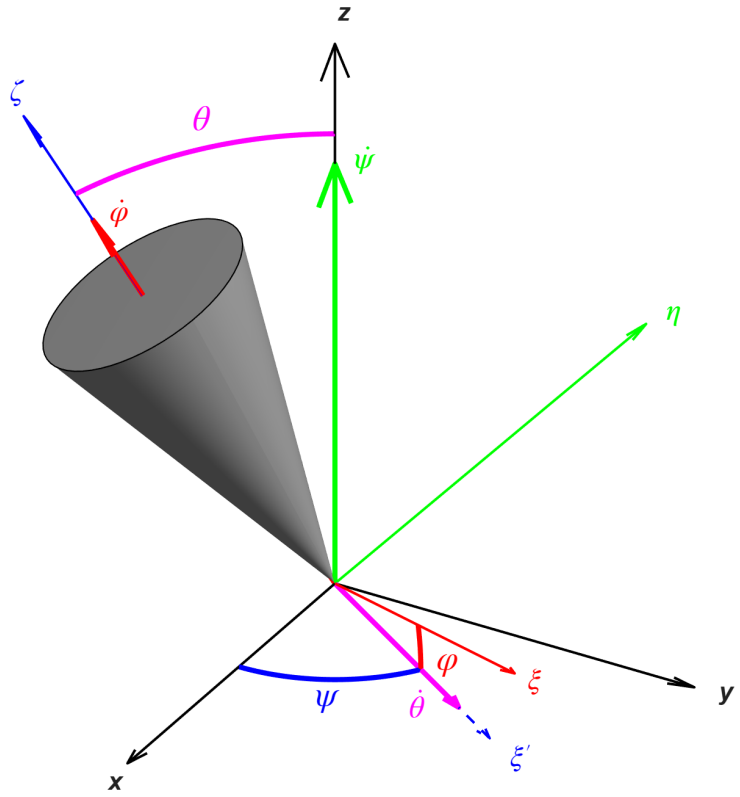
A spinning top is a rigid body performing rotational motion around a fixed point. The system is subjected to the moment of gravitational force with respect to the support point. The interaction between this moment and the angular momentum of the rotating top causes the direction of its rotation axis to change, resulting in precessional motion.
Assuming a right-handed global coordinate system xyz and a local system $\xi\eta\zeta$ with the same orientation, the top performs the following three rotational motions:

1. **Precession** (denoted by the angle ψ) is the phenomenon of changing the direction of the rigid body's rotation axis. Geometrically, it is represented as the angle between the global x-axis and the body's line of nodes $\xi\prime$. The precession angular velocity vector is aligned with the global z-axis;

2. **Nutation** (denoted by the angle θ) describes the change in the inclination of the top's symmetry axis relative to the vertical z-axis of the global frame. Thus, θ is the angle between the axes z and ζ. The direction of the nutation angular velocity lies along the line of nodes.

3. **Spin motion** (denoted by the angle φ) is the rotation about the top's own symmetry axis. It is the angle between the line of nodes and the local ξ-axis, and the corresponding angular velocity vector is parallel to the local ζ-axis.

Since the body does not undergo translational motion (the tip of the top is fixed), the system has a total of three degrees of freedom.



Rys. 5.1. Kinematic model of the spinning top. The global coordinate system is denoted by xyz, while the local coordinate system attached to the top is $\xi\eta\zeta$. The axis $\xi\prime$ represents the nodal line of the body and simultaneously the projection of the ξ axis onto the plane xy.

5.2. Analytical Solution — Euler Angles

5.2.1. System's Energy

To describe the motion of a spinning top using Euler angles, the rotation sequence $Z_\psi X_\theta Z_\varphi$ is commonly used [13]. The rotation matrix R, being the product of these matrices, can be written as:

$$R = Z_\psi X_\theta Z_\varphi = \begin{bmatrix} \cos\psi & -\sin\psi & 0 \\ \sin\psi & \cos\psi & 0 \\ 0 & 0 & 1 \end{bmatrix} \begin{bmatrix} 1 & 0 & 0 \\ 0 & \cos\theta & -\sin\theta \\ 0 & \sin\theta & \cos\theta \end{bmatrix} \begin{bmatrix} \cos\varphi & -\sin\varphi & 0 \\ \sin\varphi & \cos\varphi & 0 \\ 0 & 0 & 1 \end{bmatrix} \tag{5.1}$$

The components of the angular velocity vector are obtained by expressing the precession, nutation, and spin velocities in the local frame $\xi\eta\zeta$. The precession angular velocity $\dot{\vec{\psi}}$ is aligned with the global z-axis. Expressing this axis in the local frame yields:

$$\dot{\vec{\psi}} = \begin{bmatrix} \dot{\psi}_\xi \\ \dot{\psi}_\eta \\ \dot{\psi}_\zeta \end{bmatrix} = \begin{bmatrix} \dot{\psi}\sin\theta\sin\varphi \\ \dot{\psi}\sin\theta\cos\varphi \\ \dot{\psi}\cos\theta \end{bmatrix}. \tag{5.2}$$

The nutation angular velocity $\dot{\bar{\theta}}$ is aligned with the line of nodes ξ'. Expressing this line in the local frame gives:

$$\dot{\bar{\theta}} = \begin{bmatrix} \dot{\theta}_\xi \\ \dot{\theta}_\eta \\ \dot{\theta}_\zeta \end{bmatrix} = \begin{bmatrix} \dot{\theta}\cos\varphi \\ -\dot{\theta}\sin\varphi \\ 0 \end{bmatrix} \tag{5.3}$$

The spin angular velocity $\dot{\bar{\varphi}}$ is aligned with the local ζ-axis.

$$\dot{\bar{\varphi}} = \begin{bmatrix} 0 \\ 0 \\ \dot{\varphi} \end{bmatrix}. \tag{5.4}$$

Summing the components of precession, nutation, and spin yields the angular velocity vector expressed in the local frame:

$$\bar{\omega} = \dot{\bar{\theta}} + \dot{\bar{\psi}} + \dot{\bar{\varphi}} = \begin{bmatrix} \dot{\theta}\cos\varphi \\ -\dot{\theta}\sin\varphi \\ 0 \end{bmatrix} + \begin{bmatrix} \dot{\psi}\sin\theta\sin\varphi \\ \dot{\psi}\sin\theta\cos\varphi \\ \dot{\psi}\cos\theta \end{bmatrix} + \begin{bmatrix} 0 \\ 0 \\ \dot{\varphi} \end{bmatrix} = \begin{bmatrix} \dot{\theta}\cos\varphi + \dot{\psi}\sin\theta\sin\varphi \\ -\dot{\theta}\sin\varphi + \dot{\psi}\sin\theta\cos\varphi \\ \dot{\psi}\cos\theta + \dot{\varphi} \end{bmatrix} \tag{5.5}$$

For a symmetric top, the principal moments of inertia satisfy $I_\xi = I_\eta \neq I_\zeta$. The kinetic energy in the body-fixed frame is therefore:

$$T = \frac{1}{2} I_\xi (\dot{\xi}^2 + \dot{\eta}^2) + \frac{1}{2} I_\zeta \dot{\zeta}^2 \tag{5.6}$$

where

$$\begin{bmatrix} \dot{\xi} \\ \dot{\eta} \\ \dot{\zeta} \end{bmatrix} \coloneqq \begin{bmatrix} \dot{\theta}\cos\varphi + \dot{\psi}\sin\theta\sin\varphi \\ -\dot{\theta}\sin\varphi + \dot{\psi}\sin\theta\cos\varphi \\ \dot{\psi}\cos\theta + \dot{\varphi} \end{bmatrix} = \bar{\omega} \tag{5.7}$$

After substituting and simplifying, the kinetic energy becomes:

$$T = \frac{1}{2} I_\xi (\dot{\theta}^2 + \dot{\psi}^2 \sin^2\theta) + \frac{1}{2} I_\zeta (\dot{\varphi} + \dot{\psi}\cos\theta)^2 \tag{5.8}$$

The same expression can be obtained more directly by aligning the ξ-axis with the line of nodes $\xi\prime$, which leads to the angular velocity vector[13]:

$$\bar{\omega} = \begin{bmatrix} \dot{\theta} \\ \dot{\psi}\sin\theta \\ \dot{\varphi} + \dot{\psi}\cos\theta \end{bmatrix} \tag{5.9}$$

The potential energy of the system is:

$$V = mgl\cos\theta \tag{5.10}$$

where m is the mass of the system, g is the gravitational acceleration, and l is the distance between the system's center of mass and the origin of the coordinate frame.

5.2.2. Dynamics Equations

For the considered system, the Lagrange equations of the second kind are used. In the literature, the Lagrange equations are typically written in the form:

$$\frac{d}{dt}\frac{\partial L}{\partial \dot{q}_i} - \frac{\partial L}{\partial q_i} = Q_i \tag{5.11}$$

where $L = T - V$ is the Lagrangian, q_i denotes the generalized coordinate of the system, and Q_i is the generalized force not derived from the potential [2]. Since no non-potential forces act on the system, $Q_i = 0$.
For the analyzed system, the following generalized coordinates were adopted: $q_i = \{\psi, \theta\ \varphi\}$.

For the nutation coordinate, one obtains:

$$\frac{d}{dt}\frac{\partial L}{\partial \dot{\theta}} = I_1\ddot{\theta}, \qquad \frac{\partial L}{\partial \theta} = I_1\dot{\psi}^2 \sin\theta\cos\theta + I_3(\dot{\varphi} + \dot{\psi}\cos\theta)(-\dot{\psi}\sin\theta) - mgl\sin\theta \tag{5.12}$$

thus

$$\frac{d}{dt}\frac{\partial L}{\partial \dot{\theta}} - \frac{\partial L}{\partial \theta} = I_1\ddot{\theta} - I_1\dot{\psi}^2\sin\theta\cos\theta + I_3\dot{\psi}\sin\theta(\dot{\varphi} + \dot{\psi}\cos\theta) + mgl\sin\theta = 0 \tag{5.13}$$

Equation for Precession:

$$\begin{aligned} \frac{d}{dt}\frac{\partial L}{\partial \dot{\psi}} - \frac{\partial L}{\partial \psi} &= \frac{d}{dt}\left(I_1\dot{\psi}\sin^2\theta + I_3(\dot{\varphi} + \dot{\psi}\cos\theta)\cos\theta\right) = 0 \\ &\implies I_1\dot{\psi}\sin^2\theta + I_3(\dot{\varphi} + \dot{\psi}\cos\theta)\cos\theta = \text{const} \end{aligned} \tag{5.14}$$

And equation for Spin Motion

$$\begin{aligned} \frac{d}{dt}\frac{\partial L}{\partial \dot{\varphi}} - \frac{\partial L}{\partial \varphi} &= \frac{d}{dt}\left(I_3(\dot{\varphi} + \dot{\psi}\cos\theta)\right) = 0 \\ &\implies I_3(\dot{\varphi} + \dot{\psi}\cos\theta) = \text{const} \end{aligned} \tag{5.15}$$

After transforming the equations of motion, one obtains the following system of second-order differential equations, which can be directly implemented in the simulation model:

$$\begin{cases} \ddot{\theta} &= \dot{\psi}^2\sin\theta\cos\theta - \frac{I_3}{I_1}\dot{\psi}\sin\theta(\dot{\varphi} + \dot{\psi}\cos\theta) + \frac{mgl}{I_1}\sin\theta \\ \ddot{\psi} &= \frac{1}{I_1\sin\theta}\left(-2I_1\dot{\psi}\cos\theta\dot{\theta} + I_3\dot{\theta}(\dot{\varphi} + \dot{\psi}\cos\theta)\right) \\ \ddot{\varphi} &= -\ddot{\psi}\cos\theta + \dot{\psi}\sin\theta\dot{\theta} \end{cases} \tag{5.16}$$

In this form, the equations describe the generalized accelerations corresponding to nutation, precession, and spin motion of the top.

5.3. Analytical Solution — Quaternion Representation

In contrast to the Euler-angle-based formulation, the orientation of the spinning top is described using a single unit quaternion. This eliminates representation singularities and replaces the three Euler angles with four quaternion components satisfying the normalization condition.

The mathematical model is divided into two parts. First, the equations governing the evolution of the top's orientation are derived from quaternion kinematics. Next, using Euler's rigid-body dynamic equations, the equations describing the evolution of angular velocity are obtained.

5.3.1. Kinematic Equations

A single unit quaternion with four normalized components is sufficient to describe the orientation of the top. Since the equations of motion are second-order differential equations, the numerical model is extended by three angular-velocity components. As a result, the state vector of the numerical model consists of seven variables.

The angular-velocity vector $\bar{\omega}$ can be rewritten in quaternion form by assigning the components $\dot{\xi}, \dot{\eta}, \dot{\zeta}$ (expressed in the body-fixed frame) to the imaginary part of the quaternion and setting the real part to zero. Thus, the angular velocity and the orientation of the top can be represented by the following quaternions:

$$\bar{\omega}_q = \begin{bmatrix} 0 \\ \dot{\xi} \\ \dot{\eta} \\ \dot{\zeta} \end{bmatrix}, \quad \bar{q} = \begin{bmatrix} w \\ x \\ y \\ z \end{bmatrix} \tag{5.17}$$

Using the properties of quaternion multiplication 3.8, the real part of the product 3.22 is:

$$\mathrm{Re}(\dot{\bar{q}}) = 0 \cdot w - \bar{q} \circ \bar{\omega} = -\dot{\xi}x - \dot{\eta}y - \dot{\zeta}z \tag{5.18}$$

and the imaginary part is:

$$\mathrm{Im}(\dot{\bar{q}}) = w \begin{bmatrix} \dot{\xi} \\ \dot{\eta} \\ \dot{\zeta} \end{bmatrix} - \begin{bmatrix} \dot{\xi} \\ \dot{\eta} \\ \dot{\zeta} \end{bmatrix} \times \begin{bmatrix} x \\ y \\ z \end{bmatrix} = \begin{bmatrix} \dot{\xi}w \\ \dot{\eta}w \\ \dot{\zeta}w \end{bmatrix} - \begin{bmatrix} \dot{\eta}z - \dot{\zeta}y \\ \dot{\zeta}x - \dot{\xi}z \\ \dot{\xi}y - \dot{\eta}x \end{bmatrix} = \begin{bmatrix} \dot{\xi}w + \dot{\zeta}y - \dot{\eta}z \\ \dot{\eta}w + \dot{\xi}z - \dot{\zeta}x \\ \dot{\zeta}w + \dot{\eta}x - \dot{\xi}y \end{bmatrix} \tag{5.19}$$

This yields the final form of the quaternion derivative:

$$\dot{\bar{q}} = \frac{1}{2} \begin{bmatrix} -(\dot{\xi}x + \dot{\eta}y + \dot{\zeta}z) \\ \dot{\xi}w + \dot{\eta}z - \dot{\zeta}y \\ \dot{\eta}w + \dot{\zeta}x - \dot{\xi}z \\ \dot{\zeta}w + \dot{\xi}y - \dot{\eta}x \end{bmatrix} \tag{5.20}$$

The obtained equation describes the evolution of the top's orientation over time and constitutes the quaternion-based counterpart of the Euler-angle kinematic equations. It forms a system of four first-order

differential equations for the quaternion components. To solve it, only the current angular velocity expressed in the body-fixed frame is required. During numerical integration, this equation is solved simultaneously with the dynamic equations that provide the angular velocity derivatives. This allows the orientation of the top to be determined at every moment of the simulation without relying on Euler angles.

5.3.2. Dynamic Equations

After deriving the kinematic equations describing the evolution of orientation, it is necessary to obtain the equations governing the evolution of angular velocity. For this purpose, Euler's rigid-body dynamic equations expressed in the body-fixed frame are used. Their solution provides the angular velocity derivatives, which, together with the kinematic equations, form the complete simulation model.

The dynamics of spherical motion with a single fixed point are described by Euler's equation [2], [3]:

$$\bar{I}\dot{\bar{\omega}} + \bar{\omega} \times (\bar{I}\bar{\omega}) = \bar{M} \tag{5.21}$$

where $\bar{M}$ is the resultant external moment acting on the system, and $\bar{I}$ is the inertia tensor, which for a symmetric top expressed in the principal-axis frame is:

$$\bar{I} = \begin{bmatrix} I_\xi & 0 & 0 \\ 0 & I_\xi & 0 \\ 0 & 0 & I_\zeta \end{bmatrix} \tag{5.22}$$

Multiplying both sides by the inverse inertia matrix yields the angular-acceleration vector:

$$\dot{\bar{\omega}} = \bar{I}^{-1}\left(\bar{M} - \bar{\omega} \times (\bar{I}\bar{\omega})\right) \tag{5.23}$$

The external moment is given by:

$$\bar{M} = \bar{r} \times (m\bar{g}_b) \tag{5.24}$$

where $\bar{r} = [0, 0, l]$, and $\bar{g}_b$ is the gravitational acceleration vector expressed in the body-fixed frame. This vector can be obtained by transforming the global gravitational vector using the rotation matrix $R(\bar{q})$ [14]:

$$\bar{g}_b = R^T(\bar{q}) \cdot \bar{g} \tag{5.25}$$

where $\bar{g} = [0, 0, -g]$ and

$$R(\bar{q}) = \begin{bmatrix} 1 - 2(y^2 + z^2) & 2(xy - wz) & 2(xz + wy) \\ 2(xy + wz) & 1 - 2(x^2 + z^2) & 2(yz - wx) \\ 2(xz - wy) & 2(yz + wx) & 1 - 2(x^2 + y^2) \end{bmatrix} \tag{5.26}$$

Substituting yields:

$$\begin{aligned}\bar{g}_b = R^T(\bar{q}) \cdot \bar{g} = \begin{bmatrix} 1-2(y^2+z^2) & 2(xy+wz) & 2(xz-wy) \\ 2(xy-wz) & 1-2(x^2+z^2) & 2(yz+wx) \\ 2(xz+wy) & 2(yz-wx) & 1-2(x^2+y^2) \end{bmatrix} \begin{bmatrix} 0 \\ 0 \\ -g \end{bmatrix} = \\ = -g \begin{bmatrix} 2(xz-wy) \\ 2(yz+wx) \\ 1-2(x^2+y^2) \end{bmatrix}\end{aligned} \tag{5.27}$$

The resulting external moment is:

$$\bar{M} = \bar{r} \times (m\bar{g}_b) = \begin{bmatrix} 0 \\ 0 \\ l \end{bmatrix} \times -g \begin{bmatrix} 2(xz-wy) \\ 2(yz-wx) \\ 1-2(x^2+y^2) \end{bmatrix} = 2mgl \begin{bmatrix} wx+yz \\ wy-xz \\ 0 \end{bmatrix} \tag{5.28}$$

The cross-product term is:

$$\bar{\omega} \times (\bar{I}\bar{\omega}) = \begin{bmatrix} \dot{\xi} \\ \dot{\eta} \\ \dot{\zeta} \end{bmatrix} \times \begin{bmatrix} I_1\dot{\xi} \\ I_1\dot{\eta} \\ I_3\dot{\zeta} \end{bmatrix} = \begin{bmatrix} (I_3-I_1)\dot{\eta}\dot{\zeta} \\ (I_1-I_3)\dot{\xi}\dot{\zeta} \\ 0 \end{bmatrix} \tag{5.29}$$

Finally, combining these expressions yields the angular-acceleration vector:

$$\begin{aligned}\dot{\bar{\omega}} = \bar{I}^{-1}\left(\bar{M} - \bar{\omega} \times (\bar{I}\bar{\omega})\right) = \begin{bmatrix} I_1^{-1} & 0 & 0 \\ 0 & I_1^{-1} & 0 \\ 0 & 0 & I_3^{-1} \end{bmatrix} \begin{bmatrix} 2mgl(wx+yz) - (I_3-I_1)\dot{\eta}\dot{\zeta} \\ 2mgl(wy-xz) - (I_1-I_3)\dot{\xi}\dot{\zeta} \\ 0 \end{bmatrix} = \\ \begin{bmatrix} 2\frac{mgl}{I_1}(wx+yz) - \frac{(I_3-I_1)}{I_1}\dot{\eta}\dot{\zeta} \\ 2\frac{mgl}{I_1}(wy-xz) - \frac{(I_3-I_1)}{I_1}\dot{\xi}\dot{\zeta} \\ 0 \end{bmatrix}\end{aligned} \tag{5.30}$$

5.4. Numerical Computations

The equations of motion derived using Euler angles and quaternions were implemented in MATLAB R2025a. Both models were solved using the fourth-order Runge–Kutta method with a constant integration step of 10^{-4} [s].

The implementation of the Euler-angle model included:

1. Defining model parameters and initial conditions,
2. Computing angular accelerations from the equations of motion,
3. Converting the system to first-order differential equations,
4. Performing numerical integration using the fourth-order Runge–Kutta method,
5. Determining the time histories of angles, angular velocities, energy, and the motion trajectory.

In the quaternion-based model, the orientation of the top was represented by a unit quaternion. At each iteration, the rotation matrix, gravitational moment, angular-velocity derivative from Euler's equation, and quaternion derivative from the kinematic equation were computed, after which the resulting system was integrated using the Runge–Kutta method.
Three experiments were performed for each method:

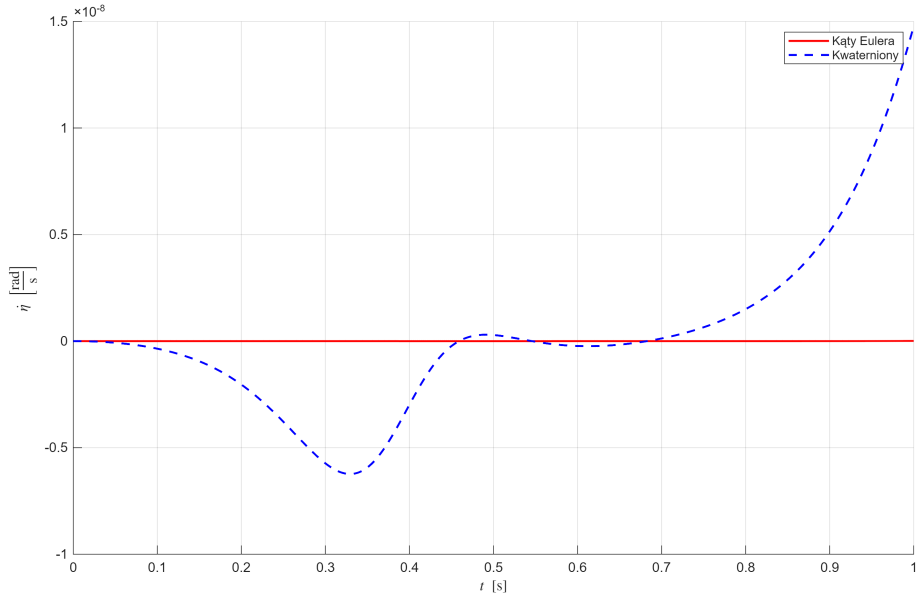
1. A perfectly vertical top with a prescribed spin velocity $\dot{\varphi} = 50 \ \left[\frac{\text{rad}}{\text{s}}\right]$,
2. A top tilted by $\theta = 5^\circ$ with the same spin velocity,
3. A top identical to experiment 2, but with zero gravitational acceleration.

Experiment 2 was used to compare both methods. The angular velocity component $\dot{\eta}$, total energy, and spatial trajectory of the top were analyzed. Additionally, the computation time was measured five times for each method, and the average value was determined.

5.4.1. Comparison of Time Histories

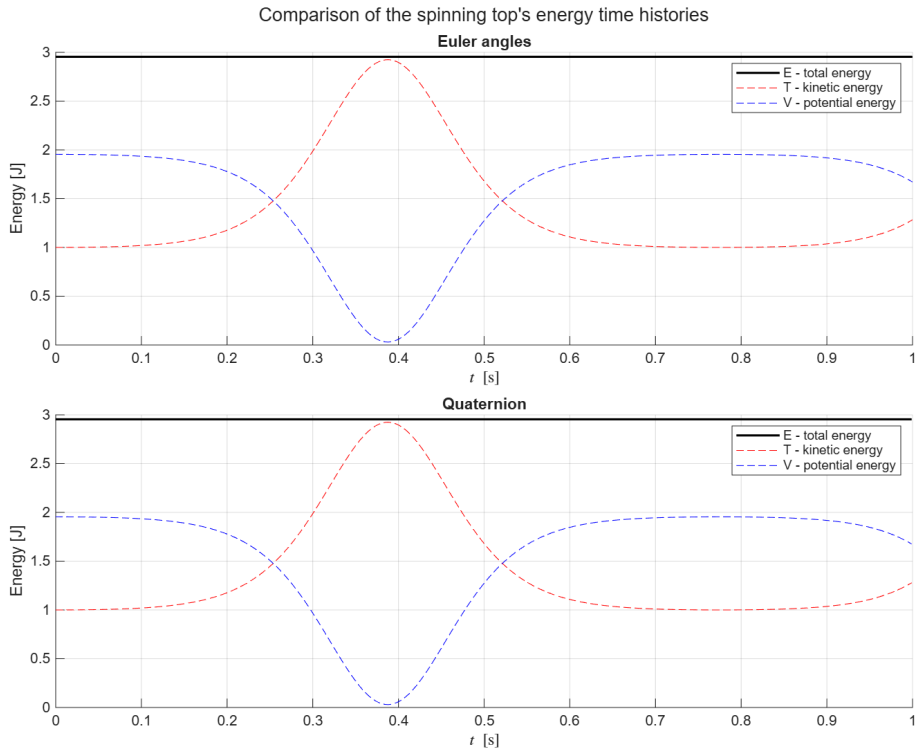
To compare both methods, the results obtained for experiment 2 were analyzed, where the initial nutation angle was $\theta_0 = 5^\circ$ and the initial spin velocity was $\dot{\varphi}_0 = 50 \ \left[\frac{\text{rad}}{\text{s}}\right]$. The angular-velocity time histories, total energy, and spatial trajectory of the top were compared. Furthermore, RMS errors between the Euler-angle and quaternion solutions were computed.

Below is a comparison of the angular-velocity time histories $\dot{\eta}$ obtained using the Euler-angle method and the quaternion-based method.



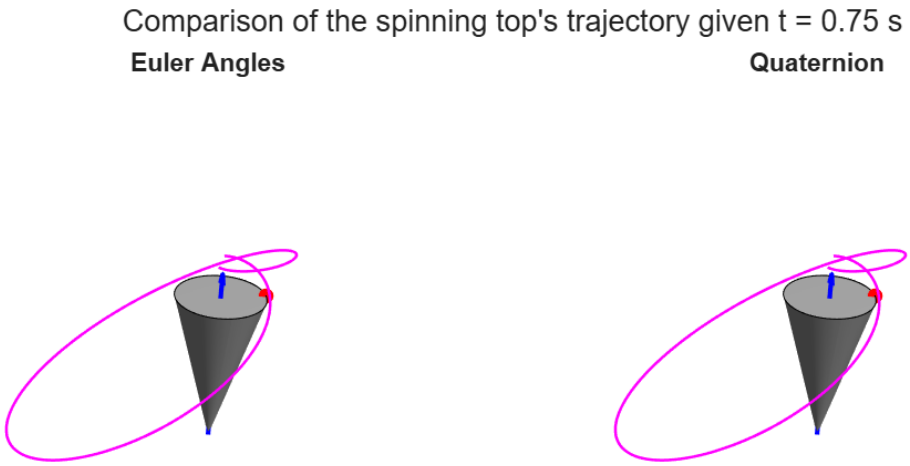
Rys. 5.2. Comparison of the angular-velocity time history $\dot{\eta}$ obtained using Euler angles and quaternions.

In order to verify the consistency of the models, the total energy time histories were also compared:



Rys. 5.3. Comparison of the top's total-energy time histories obtained using the Euler-angle method and the quaternion-based method.

Additionally, the trajectories of the tip of the top's symmetry axis obtained using both methods were compared, allowing for a qualitative assessment of the accuracy of the spatial-motion representation.



Rys. 5.4. Comparison of the trajectory of the tip of the top's symmetry axis obtained using the Euler-angle method and the quaternion-based method for experiment 2.

To quantitatively assess the agreement between the two methods, RMS errors were computed for selected quantities describing the motion of the top:

Quantity	Error type	Value
θ	Relative RMS	$7.2 \cdot 10^{-4}[\%]$
$\dot{\eta}$	Absolute RMS	$3.9 \cdot 10^{-9}\left[\frac{\text{rad}}{\text{s}}\right]$
E	Absolute RMS	$1.7 \cdot 10^{-9}[\%]$

Tabela 5.1. Indicators of agreement between the time histories obtained using the Euler-angle method and the quaternion-based method for experiment 2.

5.4.2. Comparison of Computation Time

In addition to comparing the obtained time histories, the computation time for both methods was also evaluated. The results of five consecutive measurements and their average values are presented in the table below:

Method	Computation time [s]					
	Measurement 1	MeasurementMeasurement 2	Measurement 3	Measurement 4	Measurement 5	Average
Euler angles	0.117	0.124	0.128	0.122	0.123	0.123
Quaternions	0.081	0.061	0.071	0.058	0.083	0.071
Percentage difference						42.3%

Tabela 5.2. Comparison of computation time for both numerical methods.

5.4.3. Analysis of Results

Figure 5.2 shows small differences between the time histories obtained using both methods. However, their magnitude is extremely small and cannot be clearly distinguished at the scale used in the plot. Only the quantitative analysis presented in Table 5.1 reveals that the deviations are on the order of 10^{-9}–10^{-8}, which corresponds to numerical error levels.

To quantitatively assess the agreement between the two methods, the root-mean-square (RMS) error was computed according to:

$$RMS = \sqrt{\frac{1}{N}\sum_{i=1}^{N}(x_i - y_i)^2}, \tag{5.31}$$

Where x_i and y_i denote the corresponding values obtained using the Euler-angle method and the quaternion-based method. The relative RMS error for the nutation angle was $7.2 \cdot 10^{-4}[\%]$, while the absolute RMS error for the angular velocity component $\dot{\eta}$ was only $3.9 \cdot 10^{-9}$ $\left[\frac{\text{rad}}{\text{s}}\right]$. The agreement is also visible in the energy time histories shown in Figure 5.3. The relative RMS error of the total energy was $1.7 \cdot 10^{-9}[\%]$, indicating that the differences between the methods lie at the level of numerical precision.

The consistency of both methods is further confirmed by Figure 5.4, which presents the trajectory of the tip of the top's symmetry axis. The obtained trajectories practically overlap, demonstrating that both models correctly reproduce the spatial motion.

In experiment 1, the Euler angle method led to numerical issues. For a nutation angle $\theta = 0^\circ$, the equation 5.16 contains a division by $\sin\theta$, which results in a singularity. This is a classical manifestation of gimbal lock. The quaternion-based method does not exhibit this problem.

Based on Table 5.2, it can be concluded that in the analyzed case, the quaternion model required less computation time than the Euler-angle model. The average computation time decreased from 0.123 [s] to 0.071 [s], corresponding to a reduction of approximately $42.3[\%]$. This indicates that, for the considered model, quaternions not only eliminate representation singularities but also enable efficient numerical computation.

6. Kinematics and Dynamics Modeling of a Rotor

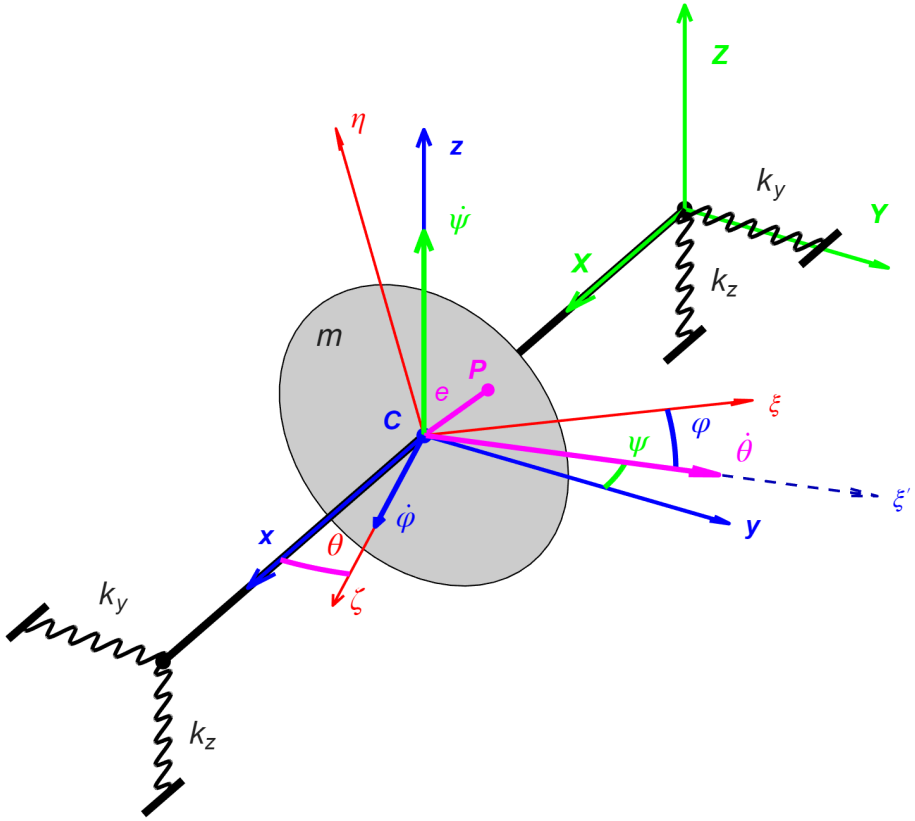
6.1. Kinematic Model of the System

The second analyzed system is an unbalanced rotor rigidly mounted on a shaft supported elastically on both sides of the disk. The rotor model follows the classical approach used in rotor dynamics, in which the shaft with the disk is described as an elastically and viscously supported system subjected to excitation resulting from mass imbalance [15]. The model uses the following three coordinate systems:

1. The global reference frame XYZ, located at one of the support points,
2. The local frame xyz, whose origin is placed at the geometric center of the rotor disk C; this frame remains parallel to the global frame and is used to describe translational motion of the rotor,
3. The local frame $\xi\eta\zeta$ is attached to the rotating rotor and is used to describe its rotational motion.

The position of the rotor is described using two translational coordinates, y_C and z_C, which represent motion perpendicular to the shaft axis; axial displacement is neglected. Similarly to the previously analyzed spinning top, the rotational motion of the rotor is described using three motions: precession, nutation, and spin. The model therefore has two translational degrees of freedom and three rotational degrees of freedom, giving a total of five degrees of freedom.

The rotor is unbalanced, so the imbalance radius e and its center P are introduced.. This imbalance generates periodic inertial forces that excite additional vibrations of the system. The shaft support points are located at distances a and b from the disk center. At the supports, stiffness coefficients k_y and k_z, and damping coefficients $b_y and b_z$ are applied along the corresponding axes.



Rys. 6.1. Kinematic model of the unbalanced rotor. The XYZ frame is the fixed reference frame associated with the shaft supports. The xyz frame is centered at the geometric center C of the rotor disk and remains parallel to the global frame. The $\xi\eta\zeta$ frame is attached to the rotor and rotates with it. Point P denotes the rotor's center of mass, offset from the geometric center C by the imbalance radius e. The axis ξ' is the projection of the ξ-axis onto the xy-plane and defines the line of nodes. The angles ψ, θ and φ describe precession, nutation, and spin, respectively. The shaft is supported at two points located at distances a and b from the disk center. In the transverse directions, elastic–damping elements with stiffness coefficients k_y, k_z and damping coefficients b_y, b_z are applied.

6.2. Analytical Solution — Euler Angles

6.2.1. Rotor Kinematics

Small angular deviations of the rotor axis from the equilibrium position are assumed:

$$|\psi| \ll 1, \qquad |\theta| \ll 1. \tag{6.1}$$

Thus, linear approximations of trigonometric functions may be used:

$$\sin\psi \approx \psi, \quad \sin\theta \approx \theta, \quad \cos\psi \approx 1, \quad \cos\theta \approx 1, \tag{6.2}$$

and second-order terms are neglected:

$$\psi^2 \approx 0, \quad \theta^2 \approx 0, \quad \psi\theta \approx 0. \tag{6.3}$$

The orientation of the $\xi\eta\zeta$ frame relative to xyz is described using the rotation matrix $\bar{Z}_\psi \bar{Y}_\theta \bar{X}_\varphi$. Additionally, the frame is rotated by $90°$ about the vertical z-axis [16]. The rotation matrix is therefore:

$$\bar{R} = \bar{Z}_\psi \bar{Y}_\theta \bar{X}_\varphi \cdot \begin{bmatrix} 0 & 0 & 1 \\ 1 & 0 & 0 \\ 0 & 1 & 0 \end{bmatrix} \tag{6.4}$$

The coordinates of point P in the global frame are expressed as the sum of its coordinates in the xyz frame and the displacement relative to XYZ:

$$\begin{bmatrix} X_P \\ Y_P \\ Z_P \end{bmatrix} = \begin{bmatrix} 0 \\ e\cos\varphi \\ e\sin\varphi \end{bmatrix} + \begin{bmatrix} l \\ y_C \\ z_C \end{bmatrix} = \begin{bmatrix} l \\ y_C + e\cos\varphi \\ z_C + e\sin\varphi \end{bmatrix} \tag{6.5}$$

The velocity of point P is the derivative of this vector:

$$\begin{bmatrix} \dot{X}_P \\ \dot{Y}_P \\ \dot{Z}_P \end{bmatrix} = \begin{bmatrix} 0 \\ \dot{y}_C - e\dot{\varphi}\sin\varphi \\ \dot{z}_C + e\dot{\varphi}\cos\varphi \end{bmatrix} \tag{6.6}$$

The angular-velocity vector in the $\xi\eta\zeta$ frame is obtained using the rotation matrix R.

$$\begin{bmatrix} \omega_\xi \\ \omega_\eta \\ \omega_\zeta \end{bmatrix} = \begin{bmatrix} \sin\varphi & \cos\varphi & 0 \\ \cos\varphi & -\sin\varphi & 0 \\ -\theta & 0 & 1 \end{bmatrix} \begin{bmatrix} \omega_\psi \\ \omega_\theta \\ \omega_\varphi \end{bmatrix} = \begin{bmatrix} \dot{\psi}\sin\varphi + \dot{\theta}\cos\varphi \\ \dot{\psi}\cos\varphi - \dot{\theta}\sin\varphi \\ -\theta\dot{\psi} + \dot{\varphi} \end{bmatrix} \tag{6.7}$$

6.2.2. Dynamics Equations

The inertia tensor of the rotor in the principal-axis frame $\xi\eta\zeta$ is:

$$\bar{I} = \begin{bmatrix} I & 0 & 0 \\ 0 & I & 0 \\ 0 & 0 & I_l \end{bmatrix} \tag{6.8}$$

Where I is the mass moment of inertia of the rotor disk about the ξ and η axes, and I_l is the moment of inertia of the shaft aligned with the ζ-axis. Based on this, the kinetic energy expressed in the $\xi\eta\zeta$ frame can be written as [16]:

$$T = \frac{1}{2}m\dot{y}_C^2 + \frac{1}{2}m\dot{z}_C^2 + \frac{1}{2}I\dot{\xi}^2 + \frac{1}{2}I\dot{\eta}^2 + \frac{1}{2}I_l\dot{\zeta}^2 + \frac{1}{2}m_P\dot{Y}_P^2 + \frac{1}{2}m_P\dot{Z}_P^2 \tag{6.9}$$

Where m_P is the mass of the imbalance point. Substituting expressions 6.6 and 6.7 yields:

$$\begin{aligned} T = \frac{1}{2}m\dot{y}_C^2 + \frac{1}{2}m\dot{z}_C^2 + \frac{1}{2}I(\dot{\psi}\sin\varphi + \dot{\theta}\cos\varphi)^2 + \frac{1}{2}I(\dot{\psi}\cos\varphi - \dot{\theta}\sin\varphi)^2 + \\ \frac{1}{2}I_l(\dot{\varphi} - \dot{\psi}\theta)^2 + \frac{1}{2}m_P(\dot{y}_C - e\dot{\varphi}\sin\varphi)^2 + \frac{1}{2}m_P(\dot{z}_C + e\dot{\varphi}\cos\varphi)^2 \end{aligned} \tag{6.10}$$

The potential energy is given by:

$$V = \frac{1}{2}k_y(y_C + \psi a)^2 + \frac{1}{2}k_y(y_C - \psi b)^2 + \frac{1}{2}k_z(z_C + \theta a)^2 + \frac{1}{2}k_z(z_C - \theta b)^2 \tag{6.11}$$

The dissipation function is:

$$N = b_y(\dot{y}_C + \dot{\psi}a)^2 + b_y(\dot{y}_C - \psi b)^2 + b_z(\dot{z}_C + \dot{\theta}a)^2 + b_z(\dot{z}_C - \theta b)^2 \tag{6.12}$$

Additionally, the system is subjected to a forcing term whose components are:

$$\bar{Q} = \begin{bmatrix} Q_x \\ Q_y \\ Q_z \end{bmatrix} = m_P e \begin{bmatrix} 0 \\ \dot{\varphi}^2\cos\varphi + \ddot{\varphi}\sin\varphi \\ \dot{\varphi}^2\sin\varphi - \ddot{\varphi}\cos\varphi \end{bmatrix} \tag{6.13}$$

The Lagrange equations of the second kind take the form:

$$\begin{cases} (m+m_P)\ddot{y}_C + 2k_y y_C + k_y(a-b)\psi + 2b_y\dot{y}_C + b_y(a-b)\dot{\psi} - m_P e(\ddot{\varphi}\sin\varphi + \dot{\varphi}^2\cos\varphi) & = 0 \\ (m+m_P)\ddot{z}_C + 2k_z z_C + k_z(a-b)\theta + 2b_z\dot{z}_C + b_z(a-b)\dot{\theta} - m_P e(\dot{\varphi}^2\sin\varphi - \ddot{\varphi}\cos\varphi) & = 0 \\ I\ddot{\psi} - I_l\dot{\varphi}\dot{\theta} + k_y y_C(a-b) + k_y(a^2+b^2)\psi + b_y\dot{y}_C(a-b) + b_y(a^2+b^2)\dot{\psi} & = 0 \\ I\ddot{\theta} + I_l\dot{\varphi}\dot{\psi} + k_z z_C(a-b) + k_z(a^2+b^2)\theta + b_y\dot{z}_C(a-b) + b_y(a^2+b^2)\dot{\theta} & = 0 \\ I_l(\ddot{\varphi} - \theta\ddot{\psi} - \dot{\theta}\dot{\psi}) - M_{zewn} & = 0 \end{cases} \tag{6.14}$$

These equations are used to determine the accelerations of the rotor's state variables.

6.3. Analytical Solution — Dual Quaternion Representation

IIn the dual quaternion-based model, the rotor's orientation is described by the real part of the dual quaternion, while the position of the geometric center of the disk is represented by its dual part. In contrast to the Euler-angle-based approach, where position and orientation are described separately using translational coordinates and angles, the dual quaternion allows both types of information to be expressed within a single algebraic structure.

The simulation model consists of two parts. The first part describes the kinematics, i.e., the method for determining the derivatives of the real and dual parts of the dual quaternion. The second part describes the dynamics, i.e., the computation of translational accelerations of the rotor center and the derivatives of angular velocity based on the forces and moments acting on the rotor.

6.3.1. Kinematic Equations of the Model

Because the system has five degrees of freedom, a single quaternion is insufficient to describe its dynamics. For this reason, a dual quaternion is used, whose algebra is presented in Section 4.2.

From equation 3.22 , the real part of the dual quaternion is:

$$\dot{\bar{q}}_r = \frac{1}{2}\bar{q}_r\bar{\omega}_q \tag{6.15}$$

and from equation 4.7, the dual part is:

$$\bar{q}_d = \frac{1}{2}\bar{r}_C\bar{q}_r \implies \dot{\bar{q}}_d = \frac{1}{2}\left(\dot{\bar{r}}_C\bar{q}_r + \bar{r}_C\dot{\bar{q}}_r\right) \tag{6.16}$$

Where $\bar{r}_C, \bar{\omega}_q$ are the quaternions corresponding to the translational displacement of the rotor center and the angular velocity of the rotor, respectively:

$$\bar{r}_C = \begin{bmatrix} 0 \\ x_C \\ y_C \\ z_C \end{bmatrix}, \quad \bar{\omega}_q = \begin{bmatrix} 0 \\ \omega_\xi \\ \omega_\eta \\ \omega_\zeta \end{bmatrix} \tag{6.17}$$

The quaternion$\bar{r}_C$ serves as the translational component of the dual quaternion in equation 6.16.

6.3.2. Rotational Motion Equations

The position of an arbitrary point D belonging to the shaft axis can be determined from:

$$\bar{r}_D = \bar{r}_C + \bar{R}\bar{\rho}_D^{(l)} \tag{6.18}$$

where $\bar{R}$ is the rotation matrix obtained from the quaternion $\bar{q}_r$ according to the relation 5.26, and $\bar{\rho}_D^{(l)}$ is the position vector of point D relative to point C, the geometric center of the rotor.
The velocity of point D is:

$$\dot{\bar{r}}_D = \dot{\bar{r}}_C + \bar{R}(\bar{\omega}_q \times \bar{\rho}_d^{(l)}) \tag{6.19}$$

Accordingly, the coordinates of the two shaft endpoints A, B can be written as:

$$\bar{\rho}_A^{(l)} = \begin{bmatrix} a \\ 0 \\ 0 \end{bmatrix}, \qquad \bar{\rho}_B^{(l)} = \begin{bmatrix} -b \\ 0 \\ 0 \end{bmatrix}. \tag{6.20}$$

The elastic–damping forces acting at the supports are described by:

$$\bar{F}_A = \begin{bmatrix} 0 \\ -k_y y_A - b_y \dot{y}_A \\ -k_z z_A - b_z \dot{z}_A \end{bmatrix}, \quad \bar{F}_B = \begin{bmatrix} 0 \\ -k_y y_B - b_y \dot{y}_B \\ -k_z z_B - b_z \dot{z}_B \end{bmatrix} \tag{6.21}$$

The displacements y_A, y_B and velocities $\dot{y}_A, \dot{y}_B$ are obtained from relations 6.18 and 6.19.
The resultant elastic–damping force is:

$$\bar{F}_s = \bar{F}_A + \bar{F}_B \tag{6.22}$$

The moment of the elastic–damping forces with respect to the rotor center is:

$$\bar{M}_s = \bar{\rho}_A^{(g)} \times \bar{F}_A + \bar{\rho}_B^{(g)} \times \bar{F}_B \tag{6.23}$$

where $\bar{\rho}_A^{(g)}, \bar{\rho}_B^{(g)}$ are the coordinates of the rotor endpoints in the global frame, expressed as:

$$\rho_A^{(g)} = R\rho_A^{(l)}, \qquad \rho_B^{(g)} = R\rho_B^{(l)}. \tag{6.24}$$

The moment of forces in the rotor-fixed frame is:

$$\bar{M}_s^{(l)} = \bar{R}^{\mathrm{T}} \bar{M}_s^{(g)}. \tag{6.25}$$

The total moment acting on the rotor is the sum of the elastic–damping moment and the driving moment:

$$\bar{M} = \bar{M}_s^{(l)} + \begin{bmatrix} M_{\mathrm{drive}} \\ 0 \\ 0 \end{bmatrix} \tag{6.26}$$

In this model, the dual quaternion is used to describe the configuration of the rotor, i.e., to simultaneously represent its orientation and translation. The dynamics equations, however, remain in the classical Newton–Euler form. This means that the dual quaternion does not replace the dynamic equations; instead, it provides the kinematic quantities required to determine position, orientation, and configuration-dependent variables.

According to the Euler equation for rigid-body dynamics 5.21, the derivative of the angular-velocity vector is:

$$\dot{\bar{\omega}} = \bar{I}^{-1} \left(\bar{M} - \bar{\omega} \times (\bar{I}\bar{\omega}) \right), \tag{6.27}$$

6.3.3. Translational Motion Equations

The position of the imbalance point relative to the rotor center is described in the local frame as:

$$\bar{r}_P^{(l)} = \begin{bmatrix} 0 \\ e\cos\varphi \\ e\sin\varphi \end{bmatrix} \tag{6.28}$$

The relative acceleration of the imbalance point in the global frame is:

$$\ddot{\bar{r}}_P^{(g)} = R\left(\dot{\bar{\omega}} \times \bar{r}_P^{(l)} + \bar{\omega} \times (\bar{\omega} \times \bar{r}_P^{(l)})\right) \tag{6.29}$$

The inertial force resulting from the imbalance is:

$$\bar{F}_u = -m_P \ddot{\bar{r}}_P^{(g)} \tag{6.30}$$

Thus, the translational motion equations of the rotor center are:

$$\ddot{y}_C = \frac{\bar{F}_{s,y} + \bar{F}_{u,y}}{m + m_P}, \qquad \ddot{z}_C = \frac{\bar{F}_{s,z} + \bar{F}_{u,z}}{m + m_P}. \tag{6.31}$$

The position of the rotor center is obtained from the dual part of the dual quaternion; however, the translational motion equations themselves follow directly from Newton's second law. The use of dual quaternions does not alter the form of these equations — it merely enables a unified representation of translation and rotation within a single mathematical structure.

6.4. Numerical Computations

To assess the correctness of the developed dual-quaternion model, a comparison was carried out between the results obtained using both methods of describing the rotor motion. The analysis was performed for two sets of initial conditions corresponding to small and large deviations of the rotor axis. Zero initial translational displacements and velocities were assumed, as well as zero initial values of the precession and spin angles and angular velocities. For both cases, the time histories of the nutation angle θ and the rotor-center displacement z_C were compared. The computation times required to perform the numerical simulations were also evaluated.

The implementation of the Euler-angle-based model proceeded through the following steps:

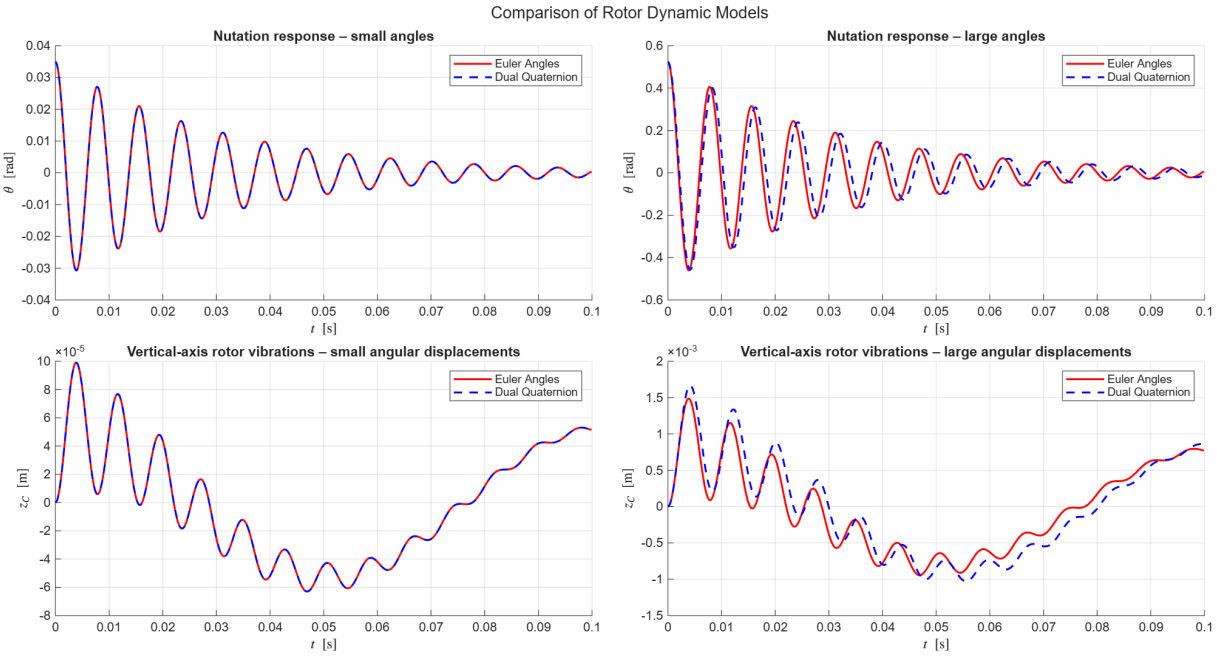
1. Definition of the model parameters and specification of the initial conditions.
2. Determination of translational and angular accelerations based on the equations of motion.
3. Transformation of the system into a set of first-order differential equations.
4. Numerical integration using the fourth-order Runge–Kutta method.
5. Computation of the time histories of displacements, velocities, and rotor orientation.

The implementation of the dual-quaternion-based model consisted of the following stages:

1. Definition of the model parameters and specification of the initial position and orientation of the rotor in the form of a dual quaternion.
2. Determination of the rotor-center position and the rotation matrix from the real and dual parts of the dual quaternion.
3. Computation of the support-point positions, elastic–damping forces, and the moments acting on the rotor.
4. Evaluation of the derivatives of the real and dual parts of the dual quaternion, the derivatives of angular velocity, and the translational accelerations.
5. Transformation of the system into a set of first-order differential equations.
6. Numerical integration using the fourth-order Runge–Kutta method.
7. Computation of the time histories of displacements and rotor orientations.

6.4.1. Comparison of Time Histories

To evaluate the consistency of both models, a comparison was performed between the time histories obtained using Euler angles and dual quaternions. The simulations were carried out for identical geometric and dynamic parameters, as well as identical initial conditions. The analysis was conducted for two values of the initial rotor-axis deviation, corresponding to small and large angular displacements. The simulation time interval was $0.1[\mathrm{s}]$, which allows for the observation of the system's transient response and assessment of the agreement between both methods in the initial phase of motion.



Rys. 6.2. Comparison of the results obtained using the Euler-angle method and the dual-quaternion method. From left to right, top to bottom: (1) Time history of the nutation angle θ for small deviations, (2) Time history of the nutation angle θ for large deviations, (3) Rotor-center displacement z_C for small deviations, (4) Rotor-center displacement z_C for large deviations.

6.4.2. Comparison of Computation Time

In addition to comparing the obtained time histories, an analysis of the computation time of both models was performed. For each method, five independent measurements of the simulation time were carried out, and their average value was then determined. The obtained results are summarized in the table below:

Method	Computation time [s]					
	Measurement 1	Measurement 2	Measurement 3	Measurement 4	Measurement 5	Average
Euler angles	0.022	0.023	0.018	0.018	0.024	0.021
Dual quaternion	0.198	0.191	0.181	0.200	0.179	0.190
Percentage difference						88.9%

Tabela 6.1. Comparison of computation time for both numerical methods.

6.4.3. Analysis of Results

Based on Figure 6.2, for small initial deviations of the rotor axis, the two methods exhibit practically complete agreement. The time histories of the nutation angle θ and the rotor-center displacement z_C overlap throughout the entire analyzed time interval. This confirms the correctness of the implementation of the dual-quaternion-based model. For larger deviations, differences between the solutions become visible, resulting from the approximations used in the Euler-angle-based model. These discrepancies arise because the Euler-angle model was derived under the assumption of small angles, whereas in the dual-quaternion model, the rotor orientation is computed directly from the quaternion.

However, it should be noted that, in the analyzed case, the computation time favors the Euler-angle-based model. From Table 6.1, it follows that the computation time required to perform the simulation using the dual-quaternion model is, on average, nearly nine times greater than that for the Euler-angle model. This means that the more accurate representation of rotor motion is obtained at the cost of significantly higher computational complexity.

7. Summary

The conducted analyses confirmed that both the classical description of rigid-body motion using Euler angles and the formulations based on quaternions and dual quaternions allow for correct modeling of the systems under consideration. For both developed models, a very high agreement of numerical results was obtained, which validates the correctness of the derived equations and their implementation in MATLAB. The analysis of the top model demonstrated that the quaternion representation eliminates the gimbal-lock problem present in the Euler-angle formulation. At the same time, the performed tests yielded shorter computation times compared to the classical model. This indicates that, for spherical motion, quaternions provide not only a more universal but also a computationally efficient method for describing orientation. In the case of the unbalanced rotor model, the use of dual quaternions enabled the simultaneous description of rotational and translational motion within a single mathematical representation. The obtained results were consistent with those produced by the classical method, while the longer computation time resulted from the more general model, which does not rely on the simplifications present in the Euler-angle-based solution.

The analyses carried out show that quaternions and dual quaternions constitute a valuable alternative to classical methods of describing rigid-body motion. Their use eliminates problems associated with representation singularities and provides a unified description of spatial motion, which is particularly important in rotor-machine modeling, robotics, space technologies, and other fields requiring precise representation of object orientation and position.

Based on the obtained results, it can be concluded that the objective of the thesis has been achieved. The study demonstrated the feasibility of effectively using quaternions and dual quaternions for modeling rigid-body motion, and the comparison made it possible to identify their advantages and limitations relative to the classical Euler-angle-based approach.

Bibliografia

[1] Jan Misiak. *Mechanika ogólna*. Wydawnictwa Naukowo-Techniczne, 1989.

[2] Goldstein H., Poole C. P. i Safko J. L. *Classical mechanics, third edition*. Pearson, 2011.

[3] Schaub H. i Junkins J. L. *Analytical mechanics of space systems, fourth edition*. AIAA Education Series, 2028.

[4] Dam E. B, Koch M. i Lillholm M. *Quaternions, Interpolation and Animation*. Sprawozdanie techniczne. Department of Computer Science, University of Copenhagen, 1998.

[5] Ben Kenwright. „A Beginners Guide to Dual-Quaternions. What They Are, How They Work, and How to Use Them for 3D Character Hierarchies". W: *International Conference in Central Europe on Computer Graphics and Visualization* (2012).

[6] McDonald J. „Teaching Quaternions is not Complex". W: *EUROGRAPHICS* (2009).

[7] Basile Graf. *Quaternions and Dynamics*. Sprawozdanie techniczne. Manuscript, EPFL. 2007.

[8] Schwab Arend. L. *Quaternions, Finite Rotation and Euler Parameters*. Sprawozdanie techniczne. Laboratory for Engineering Mechanics Delft University of Technology, 2002.

[9] J. G. Farias, E. De Pieri i Martins D. „A Review on the Applications of Dual Quaternions". W: *Machines* 12.402 (2024).

[10] Valverde A. i Tsiotras P. „Dual Quaternion Framework for Modeling of Spacecraft-Mounted Multibody Robotic Systems". W: *frontiers in Robotics and AI* (2018).

[11] Valverde A. i Tsiotras P. „Spacecraft Robot Kinematics Using Dual Quaternions". W: *robotics* (2018).

[12] Challis John. H. „Quaternions as a solution to determining the angular kinematics of human movement". W: *BMC Biomedical Engineering* (2020, 2:5).

[13] L. Landau i E. Lifszic. *Mechanika*. Państwowe Wydawnictwo Naukowe, 1961.

[14] Jack B. Kuipers. *Quaternions and rotations sequences*. Princeton University Press, 1999.

[15] Erwin Krämer. *Dynamics of rotors and foundations*. pringer-Verlag Berlin Heidelberg GmbH, 1993.

[16] Cieplok G. i Wójcik K. „Conditions for self-synchronization of inertial vibrators of vibratory conveyors in general motion". W: *Journal of theoretical and applied mechanics* (2020).